Dyes and Pigments 95 (2012) 606–613

Contents lists available at SciVerse ScienceDirect

Dyes and Pigments

journal homepage: www.elsevier.com/locate/dyepig

Design and synthesis of rhodamine based chemosensors for the detection of Fe^{3+} ions

Narendra Reddy Chereddy [a], Koorathota Suman [a], Purna Sai Korrapati [b], Sathiah Thennarasu [a,*], Asit Baran Mandal [c,**]

[a] Organic Chemistry Division, CSIR-Central Leather Research Institute, Adyar, Chennai 600 020, India
[b] Biomaterials Laboratory, CSIR-Central Leather Research Institute, Adyar, Chennai 600 020, India
[c] Chemical Laboratory, CSIR-Central Leather Research Institute, Adyar, Chennai 600 020, India

ARTICLE INFO

Article history:
Received 9 February 2012
Received in revised form
20 May 2012
Accepted 21 May 2012
Available online 9 July 2012

Keywords:
Rhodamine
Chemosensors
Fe^{3+} selectivity
Size of chelating cavity
Naked eye detection
Live cell imaging

ABSTRACT

The number and nature of coordinating entities as well as the size of chelating cavity in rhodamine based chemosensors were tuned to enhance the selectivity and sensitivity for Fe^{3+} ions. An intense pink color development and enhancement in fluorescence emission intensity of chemosensor **5** upon complex formation at pH 7·4 enabled the detection of Fe^{3+} ions in the presence of other competitive metal ions like Li^{+}, Na^{+}, K^{+}, Cs^{+}, Mg^{2+}, Ca^{2+}, Sr^{2+}, Cr^{3+}, Mn^{2+}, Fe^{2+}, Cu^{2+}, Co^{2+}, Ni^{2+}, Zn^{2+}, Cd^{2+}, Hg^{2+}, and Pb^{2+}. A plausible application of chemosensor **5** in the imaging of live fibroblast cells exposed to Fe^{3+} ions is also demonstrated.

1. Introduction

Selective detection of Fe^{3+} assumes importance because iron plays an important role in cellular metabolism [1] and enzyme catalysis [2–4]. Iron is an essential trace element for both plants and animals, including humans. Consequently, deficiency in Fe^{3+} leads to anemia, liver and kidney damages, diabetes, and heart diseases [5]. Several techniques like atomic absorption spectroscopy [6], colorimetry [7], spectrophotometry [8–10], and voltammetry [11] have been developed for Fe^{3+} detection, but these require sophisticated equipments, tedious sample preparation procedures, and trained analysts. Therefore, chemosensors which allow naked-eye detection, have advantages over other methods in being easy to operate, portable, and not requiring sophisticated instrumentation.

Rhodamine is one of the most attractive fluorochromes because of its photo physical properties [12]. Recently, much effort has been focused on the development of rhodamine based chemosensors [13–17] and polymeric chemosensors [18,19] for the detection of heavy metal ions. However, only a few chemosensors are available in literature for Fe^{3+} detection [20–48], and some of the chemosensors developed for selective detection of Fe^{3+} suffer from cross-sensitivity toward competitive metal ions like Cu^{2+} and Cr^{3+} [41–48]. Hence, a chemosensor that detects Fe^{3+} even in the presence of high concentrations of Cu^{2+} and Cr^{3+} would be more attractive. Since Fe^{3+} is a fluorescence quencher because of its paramagnetic nature [49], development of chemosensors that exhibit fluorescence enhancement upon binding with Fe^{3+} would be very much attractive. According to the theory of hard and soft acids and bases (HSAB theory), a stable complex is formed between a hard base and a hard acid such as Fe^{3+} ions. This theory offers a possibility to develop ligands with improved selectivity toward a particular metal ion depending upon the strengths of hard and soft acids and bases. The nature and number of the external chelating moieties incorporated with the rhodamine [41,50] play an important role for tuning metal ion selectivity. We used these advantages for developing new chemosensors that show selectivity for a single metal ion of interest over other competitive metal ions.

For the present study, we synthesized six rhodamine based chemosensors by subtly changing the number, nature and size of the coordinating entities. **5** showed the highest degree of sensitivity and

* Corresponding author. Tel.: +91 44 24913289; fax: +91 44 24911589.
** Corresponding author.
E-mail addresses: thennarasu@gmail.com (S. Thennarasu), abmandal@clri.res.in (A.B. Mandal).

0143-7208/$ – see front matter © 2012 Elsevier Ltd. All rights reserved.
http://dx.doi.org/10.1016/j.dyepig.2012.05.025

selectivity for Fe^{3+} over Cu^{2+} as compared with the other five analogs. The selectivity and sensitivity of **5** for Fe^{3+} were exploited for the detection of live fibroblast cells exposed to Fe^{3+} ions.

2. Experimental section

2.1. General

Dry acetonitrile and double distilled water were used throughout the experiment. All the materials for synthesis were purchased from commercial suppliers and used without further purification. The solutions of metal ions were prepared from the corresponding chloride salts. Absorption spectra were recorded on a CARY BIO 50 UV–VIS spectrophotometer. Fluorescence measurements were performed on a Perkin Elmer LC 45 Luminescence spectrometer. All pH measurements were made with a Systronics μpH System Model 361. NMR spectra were recorded using a JEOL –ECP500 MHz spectrometer operated at 500 MHz. ESI MS spectra were obtained on a HP 1100 LC-MS Analyzer without using the LC part. Fluorescence imaging experiments were performed using Olympus CK 40 Fluorescence Microscope. All measurements were carried out at room temperature (~298 K).

2.1.1. Synthesis of rhodamine hydrazide

Rhodamine hydrazide was synthesized following the reported procedure [31]. To rhodamine B hydrochloride (0.96 g, 2 mmol) dissolved in 15 mL methanol, excess amount of hydrazine hydrate (1 mL, 6.98 mmol) was added and the reaction mixture was refluxed till the pink color disappeared (~3–4 h). After that, the reaction mixture was cooled to room temperature, poured into distilled water and extracted with ethylacetate (6 × 25 mL). The combined extract was washed with brine, dried with anhydrous sodium sulfate, filtered, and then concentrated under reduced pressure to yield 0.62 g (68%) of rhodamine hydrazide.

^{1}H NMR ($CDCl_3$, 500 MHz): δ 1.16 (t, J = 7.5 Hz, 12H, $NCH_2\underline{CH_3}$), 3.32 (q, J = 6.8 Hz, 8H, $N\underline{CH_2}CH_3$), 3.63 (bs, 2H, NH_2), 6.28 (dd, J = 2.3 Hz, 2H, Xanthene–H), 6.43 (d, J = 2.3 Hz, 2H, Xanthene–H), 6.45 (d, J = 9.2 Hz, 2H, Xanthene–H), 7.10 (m, 1H, Ar–H), 7.44 (t, J = 3.5 Hz, 2H, Ar–H), 7.93 (m, 1H, Ar–H); ^{13}C NMR ($CDCl_3$, 125 MHz): δ 12.7, 44.5, 66.0, 98.0, 104.5, 108.1, 123.1, 123.9, 128.1, 128.2, 130.1, 132.6, 148.9, 151.6, 153.9, 166.3.

2.1.2. Synthesis chemosensor **1**

To a solution of rhodamine hydrazide (0.46 g, 1 mmol) dissolved in 20 mL methanol, pyridine-2-aldehyde (0.11 g, 1 mmol) was added. The red color mixture thus obtained was refluxed in an oil bath for 3 h. After that, the solution was cooled to room temperature. The resultant mixture was subjected to silica gel 100–200 mesh column chromatography using 1:3 hexane-ethtylacetate as eluent to yield 0.40 g (75%) of **1** as colorless solid.

^{1}H NMR ($CDCl_3$, 500 MHz): δ 1.14 (12H, t, J = 6.9 Hz, $NCH_2\underline{CH_3}$), 3.29 (8H, q, J = 6.9 Hz, $N\underline{CH_2}CH_3$), 6.25 (2H, d, J = 2.3 Hz, Xanthene–H), 6.41 (2H, d, J = 3.0 Hz, Xanthene–H), 6.54 (1H, d, J = 9.1 Hz, Xanthene–H), 7.11 (2H, m, Ar–H, imine–H), 7.46 (2H, m, Ar–H), 7.60 (1H, d, J = 6.9 Hz, pyridine–H), 8.00 (1H, t, J = 6.9 Hz, pyridine–H), 8.34 (1H, s, Ar–H), 8.45 (1H, d, J = 4.6 Hz, pyridine–H); ^{13}C NMR ($CDCl_3$, 125 MHz): δ 12.7, 44.4, 65.9, 98.3, 105.5, 108.1, 120.8, 123.7, 123.8, 127.7, 128.0, 128.3, 133.9, 136.3, 145.7, 149.0, 149.1, 152.6, 152.9, 154.5, 165.7.

ESI-MS: calcd for $C_{34}H_{35}N_5O_2$ m/z (M^+) 545.3, found $(M + H)^+$ 546.4.

2.1.3. Synthesis chemosensor **2**

Rhodamine hydrazide (0.46 g, 1 mmol) was dissolved in 20 mL methanol and furan-2-aldehyde (0.10 g, 1 mmol) was added. Upon addition red color developed immediately. Then the mixture was refluxed in an oil bath for 3 h. After that, the solution was cooled to room temperature. The resultant mixture was subjected to silica gel 100–200 mesh column chromatography using 1:3 hexane-ethtylacetate as eluent to get 0.395 g (74%) of **2** in pure form as colorless solid.

^{1}H NMR ($CDCl_3$, 500 MHz): δ 1.15 (12H, t, J = 6.9 Hz, $NCH_2\underline{CH_3}$), 3.31 (8H, q, J = 6.9 Hz, $N\underline{CH_2}CH_3$), 6.25 (2H, d, J = 2.3 Hz, Xanthene–H), 6.35 (1H, s, furan–H), 6.41 (2H, d, J = 2.3 Hz, Xanthene–H), 6.54 (2H, d, J = 9.1 Hz, Xanthene–H), 6.59 (1H, s, furan–H), 7.05 (1H, d, J = 6.9 Hz, Ar–H), 7.37 (1H, s, imine–H), 7.44 (2H, m, Ar–H), 7.98 (1H, d, J = 6.9 Hz, furan–H), 8.17 (2H, s, Ar–H); ^{13}C NMR ($CDCl_3$, 125 MHz): δ 12.7, 12.8, 44.4, 65.7, 98.0, 105.5, 108.2, 111.6, 112.3, 123.5, 123.6, 127.9, 128.1, 128.3, 133.6, 136.0, 143.9, 149.1, 150.7, 152.6, 152.9, 165.3.

ESI-MS: calcd for $C_{33}H_{34}N_4O_3$ m/z (M^+) 534.3, found $(M + H)^+$ 535.4.

2.1.4. Synthesis of bis-salicylaldehyde derivatives (***A, B, C*** and ***D***)

Salicylaldehyde (5.0 mmol, 0.61 g) was dissolved in 20 mL DMF, and potassium corbonate (12.5 mmol, 1.73 g) was added and the mixture was stirred at room temperature. Methelenebromide (2.5 mmol, 0.44 g), 1,2- dibromoethane (2.5 mmol, 0.47 g), 1,3-dibromopropane (2.5 mmol, 0.51 g) or 1,4- dibromobutane (2.5 mmol, 0.55 g) was added drop wise and then the mixture was stirred under reflux for 6 h. The resultant mixture was partitioned between water and ethylacetate, ethylacetate layer was collected, concentrated under reduced pressure and then subjected to silica gel 100–200 mesh column chromatography using 1:9 hexane-ethtylacetate as eluent to afford compounds **A** (0.96 g, 75%), **B** (0.97 g, 72%), **C** (1.07 g, 75%) and **D** (1.17 g, 75%) in pure form.

*2.1.4.1. NMR data of bis-salicylaldehyde (**A**).* ^{1}H NMR ($CDCl_3$, 500 MHz): δ 6.01 (2H, s, $O\underline{CH_2}O$), 7.17 (2H, t, J = 6.9 Hz, Ar–H), 7.37 (2H, d, J = 8.4 Hz, Ar–H), 7.61 (2H, t, J = 8.4 Hz, Ar–H), 7.86 (2H, dd, J = 1.6 Hz, Ar–H), 10.46 (2H, s, Aldehyde–H); ^{13}C NMR ($CDCl_3$, 125 MHz): δ 90.7, 115.0, 123.1, 125.8, 129.0, 136.1, 158.7, 189.2.

*2.1.4.2. NMR data of bis-salicylaldehyde (**B**).* ^{1}H NMR ($CDCl_3$, 500 MHz): δ 4.52 (4H, s, $O\underline{CH_2}\underline{CH_2}O$), 7.06 (4H, m, Ar–H), 7.57 (2H, t, J = 7.6 Hz, Ar–H), 7.82 (2H, d, J = 6.2 Hz, Ar–H), 10.43 (2H, s, Aldehyde–H); ^{13}C NMR ($CDCl_3$, 125 MHz): δ 67.1, 112.9, 121.5, 125.2, 128.6, 136.1, 160.9, 189.5.

*2.1.4.3. NMR data of bis-salicylaldehyde (**C**).* ^{1}H NMR ($CDCl_3$, 500 MHz): δ 2.43 (2H, p, $OCH_2\underline{CH_2}CH_2O$), 4.33 (4H, t, J = 7.6 Hz, $O\underline{CH_2}CH2\underline{CH_2}O$), 7.03 (4H, m, Ar–H), 7.55 (2H, t, J = 7.7 Hz, Ar–H), 7.83 (2H, d, J = 7.7 Hz, Ar–H), 10.49 (2H, s, Aldehyde–H); ^{13}C NMR ($CDCl_3$, 125 MHz): δ 29.2, 64.7, 112.5, 121.0, 124.9, 128.8, 136.2, 161.0, 189.6.

*2.1.4.4. NMR data of bis-salicylaldehyde (**D**).* ^{1}H NMR ($CDCl_3$, 500 MHz): δ 2.10 (4H, s, $OCH_2\underline{CH_2}\underline{CH_2}CH_2O$), 4.19 (4H, s, $O\underline{CH_2}CH_2CH_2\underline{CH_2}O$), 6.98 (4H, m, Ar–H), 7.52 (2H, t, J = 6.9 Hz, Ar–H), 7.83 (2H, d, J = 6.9 Hz, Ar–H), 10.49 (2H, s, Aldehyde-H); ^{13}C NMR ($CDCl_3$, 125 MHz): δ 26.0, 67.9, 112.5, 121.0, 124.9, 128.6, 136.1, 161.2, 189.7.

2.1.5. Synthesis of bis-rhodamine chemosensors ***3, 4, 5*** and ***6***

Rhodamine hydrazide (0.46 g, 1 mmol) was dissolved in 20 mL methanol, and bis-salicylaldehyde derivative **A** (0.13 g, 0.5 mmol), **B** (0.14 g, 0.5 mmol), **C** (0.15 g, 0.5 mmol) or **D** (0.16 g, 0.5 mmol) was added. The mixture was refluxed in an oil-bath for ~3 h and then cooled to room temperature. The resultant mixture was subjected to silica gel 100–200 mesh column chromatography using 1:3

hexane-ethtylacetate as eluent to afford **3** (0.425 g, 75%), **4** (0.435 g, 75%),**5** (0.44 g, 75%) and **6** (0.45 g, 75%) as colorless solids.

*2.1.5.1. NMR and Mass analytical data of chemosensor **3**.* ^{1}H NMR ($CDCl_3$, 500 MHz): δ 1.08 (24H, t, J = 7.5 Hz, $NCH_2\underline{CH_3}$), 3.24 (16H, q, J = 6.9 Hz, $N\underline{CH_2}CH_3$), 5.29 (2H, s, $O\underline{CH_2}O$), 6.22 (4H, dd, J = 2.3 Hz, Xanthene–H), 6.41 (4H, d, J = 2.3 Hz, Xanthene–H), 6.53 (4H, d, J = 9.2 Hz, Xanthene–H), 7.00 (2H, t, J = 7.5 Hz, Ar–H), 7.08 (2H, d, J = 6.9 Hz, Ar–H), 7.12 (2H, d, J = 8.6 Hz, Ar–H), 7.39 (2H, t, J = 7.5 Hz, Ar–H), 7.45 (4H, p, J = 7.5 Hz, Ar–H), 7.93 (2H, d, J = 6.9 Hz, Ar–H), 8.01 (2H, d, J = 6.9 Hz, Ar–H), 8.67 (2H, s, imine–H); ^{13}C NMR ($CDCl_3$, 125 MHz): δ 12.7, 44.4, 65.7, 91.6, 97.9, 105.7, 108.2, 114.7, 122.4, 123.5, 123.8, 124.7, 126.6, 128.1, 128.3, 128.7, 131.1, 133.5, 141.9, 149.0, 152.5, 153.0, 156.0, 165.3.

ESI MS: calcd for $C_{71}H_{72}N_8O_6$ m/z (M^+) 1132.4, found $(M + H)^+$ 1133.3.

*2.1.5.2. NMR and Mass analytical data of chemosensor **4**.* ^{1}H NMR ($CDCl_3$, 500 MHz): δ 1.03 (24H, t, J = 7.5 Hz, $NCH_2\underline{CH_3}$), 3.20 (16H, q, J = 4.6 Hz, $N\underline{CH_2}CH_3$), 4.19 (4H, s, $O\underline{CH_2}\underline{CH_2}O$), 6.21 (4H, dd, J = 2.3 Hz, Xanthene–H), 6.39 (4H, d, J = 2.9 Hz, Xanthene–H), 6.54 (4H, d, J = 9.2 Hz, Xanthene–H), 6.95 (2H, t, J = 7.5 Hz, Ar–H), 7.00 (2H, d, J = 8.6 Hz, Ar–H), 7.06 (2H, d, J = 6.9 Hz, Ar–H), 7.31 (2H, t, J = 8.1 Hz, Ar–H), 7.45 (4H, p, J = 7.5 Hz, Ar–H), 8.02 (4H, t, J = 6.9 Hz, Ar–H), 8.69 (2H, s, imine–H); ^{13}C NMR ($CDCl_3$, 125 MHz): δ 12.6, 44.4, 65.6, 66.3, 97.8, 105.6, 108.2, 112.4, 121.4, 123.5, 123.8, 124.3, 126.5, 128.2, 128.3, 128.8, 131.0, 133.5, 141.4, 149.0, 152.6, 152.9, 157.1, 165.3.

ESI MS: calcd for $C_{72}H_{74}N_8O_6$ m/z (M^+) 1146.4, found $(M + H)^+$ 1147.5.

*2.1.5.3. NMR and Mass analytical data of chemosensor **5**.* ^{1}H NMR ($CDCl_3$, 500 MHz): δ 1.07 (24H, t, J = 7.5 Hz, $NCH_2\underline{CH_3}$), 2.05 (2H, p, J = 6.3 Hz, $OCH_2\underline{CH_2}CH_2O$), 3.22 (16H, q, J = 7.5 Hz, $N\underline{CH_2}CH_3$), 3.99 (4H, s, $O\underline{CH_2}CH_2\underline{CH_2}O$), 6.22 (4H, dd, J = 2.3 Hz, Xanthene–H), 6.41 (4H, d, J = 1.7 Hz, Xanthene–H), 6.56 (4H, d, J = 9.2 Hz, Xanthene–H), 6.85 (4H, m, Ar–H), 7.04 (2H, d, J = 6.9 Hz, Ar–H), 7.20 (2H, t, J = 7.5 Hz, Ar–H), 7.40 (4H, p, J = 7.5 Hz, Ar–H), 7.95 (2H, d, J = 8.1 Hz, Ar–H), 7.98 (2H, d, J = 6.3 Hz, Ar–H), 8.81 (2H, s, imine-H); ^{13}C NMR ($CDCl_3$, 125 MHz): δ 12.8, 29.6, 44.4, 64.9, 65.7, 98.0, 106.0, 108.2, 112.1, 120.7, 123.5, 123.7, 124.0, 126.5, 127.9, 128.3, 128.5, 131.0, 133.5, 142.5, 148.9, 152.6, 152.9, 157.6, 165.3. ESI MS: calcd for $C_{73}H_{76}N_8O_6$ m/z (M^+) 1160.4, found $(M + H)^+$ 1161.5.

*2.1.5.4. NMR and Mass analytical data of chemosensor **6**.* ^{1}H NMR ($CDCl_3$, 500 MHz): δ 1.09 (24H, t, J = 6.9 Hz, $NCH_2\underline{CH_3}$), 1.91 (4H, s, $OCH_2\underline{CH_2}\underline{CH_2}CH_2O$), 3.27 (16H, q, J = 6.9 Hz, $N\underline{CH_2}CH_3$), 3.93 (4H, s, $O\underline{CH_2}CH_2CH_2\underline{CH_2}O$), 6.22 (4H, dd, J = 2.3 Hz, Xanthene–H), 6.41 (4H, d, J = 2.3 Hz, Xanthene–H), 6.55 (4H, d, J = 9.2 Hz, Xanthene–H), 6.77 (2H, d, J = 8.0 Hz, Ar–H), 6.86 (2H, t, J = 7.5 Hz, Ar–H), 7.08 (2H, d, J = 6.9 Hz, Ar–H), 7.19 (2H, t, J = 8.0 Hz, Ar–H), 7.44 (4H, p, J = 7.5 Hz, Ar–H), 7.95 (2H, d, J = 6.9 Hz, Ar–H), 7.99 (2H, d, J = 7.5 Hz, Ar–H), 8.81 (2H, s, imine–H); ^{13}C NMR ($CDCl_3$, 125 MHz): δ 12.7, 25.8, 44.4, 65.8, 67.7, 98.0, 106.1, 108.2, 112.0, 120.7, 123.4, 123.7, 124.1, 126.4, 127.9, 128.3, 128.9, 131.0, 133.4, 142.7, 148.9, 152.4, 153.0, 157.6, 165.2.

ESI MS: calcd for $C_{74}H_{78}N_8O_6$ m/z (M^+) 1174.4, found $(M + H)^+$ 1175.5.

2.2. Preparation of solutions for absorption and fluorescence measurements

Stock solutions of chemosensors were prepared by dissolving the required amounts of chemosensors (5.46 mg, 5.35 mg, 11.33 mg, 11.47 mg, 11.61 mg and 11.75 mg of chemosensors **1**, **2**, **3**, **4**, **5** and **6** respectively, 1.0 mmol) in 1:1 v/v 0.01 M Tris HCl–CH_3CN (pH 7·4) and making up to the mark in a 10 mL volumetric flask. Further dilutions were made to prepare 100 μM solutions for the experiments. To 1.0 mL of this solution in a 10 mL volumetric flasks was added 9.0 mL 1:1 v/v 0.01 M Tris HCl–CH_3CN (pH 7·4) containing different concentrations of metal ions, so as to get an overall dye concentration of 10 μM for the experiments. Absorption and fluorescence measurements were made using a 3.0 mL cuvette.

3. Results and discussion

Rhodamine hydrazide was prepared as described previously [51]. Chemosensors **1** and **2** were facilely synthesized by the condensation of rhodamine hydrazide with pyridine-2-aldehyde and furan-2-aldehyde, respectively, as shown in Scheme 1, and characterized by NMR and Mass analyses (Supporting data, Fig. S3–S8). The existence of spirocyclic ring structure in **1** and **2** were confirmed by the observation of ^{13}C NMR resonances at ~65.88 and ~65.66 ppm, respectively (Supporting data, Fig. S4 and S6). Although both **1**and **2** contain the rhodamine moiety, they were colorless in 0.01 M Tris HCl–CH_3CN mixture (pH 7.4) as well as in other organic solvents confirming the existence of the ring-closed spirolactam as the predominant species [52]. The limited solubility of rhodamine derivatives in water and aqueous buffer necessitated the use of other organic solvents miscible with water. Between CH_3CN and MeOH, the two organic solvents highly miscible with water, the rhodamine derivatives **1** and **2** were more soluble in CH_3CN than in MeOH. On studying the absorbance properties of **1** and **2** in aqueous buffer containing different proportions of CH_3CN, we inferred that the 1:1 mixture of aqueous buffer and CH_3CN would contain the minimum amount of organic solvent and display excellent solubility of rhodamine derivatives. The absorbance and fluorescence characteristics of **1** and **2** were greatly influenced by the addition of Cu^{2+} or Fe^{3+} ions. A clear pink color with a good fluorescence emission developed (Supporting data, Fig. S9) upon addition of 50 μM concentrations of either Cu^{2+} or Fe^{3+} ions, while other competitive metal ions (Li^+, Na^+, K^+, Cs^+, Mg^{2+}, Ca^{2+}, Sr^{2+}, Cr^{3+}, Mn^{2+}, Fe^{2+}, Co^{2+}, Ni^{2+}, Zn^{2+}, Cd^{2+}, Hg^{2+}, and Pb^{2+}) showed negligible effect. The UV–Visible absorption spectrum of **1** and **2** are shown in the Fig. S10 (Supporting data). The 10 μM solutions of **1** and **2** in 1:1 v/v 0.01 M Tris

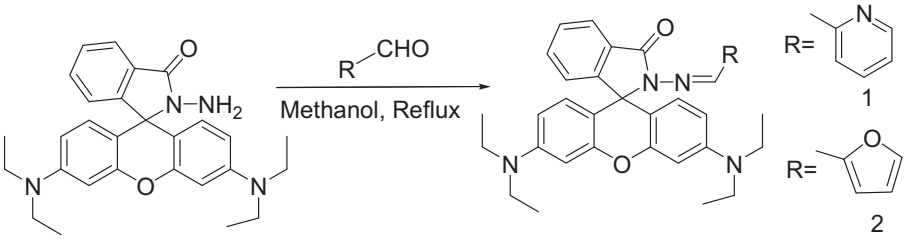

Scheme 1. Synthesis of rhodamine based chemosensors **1**–**2**.

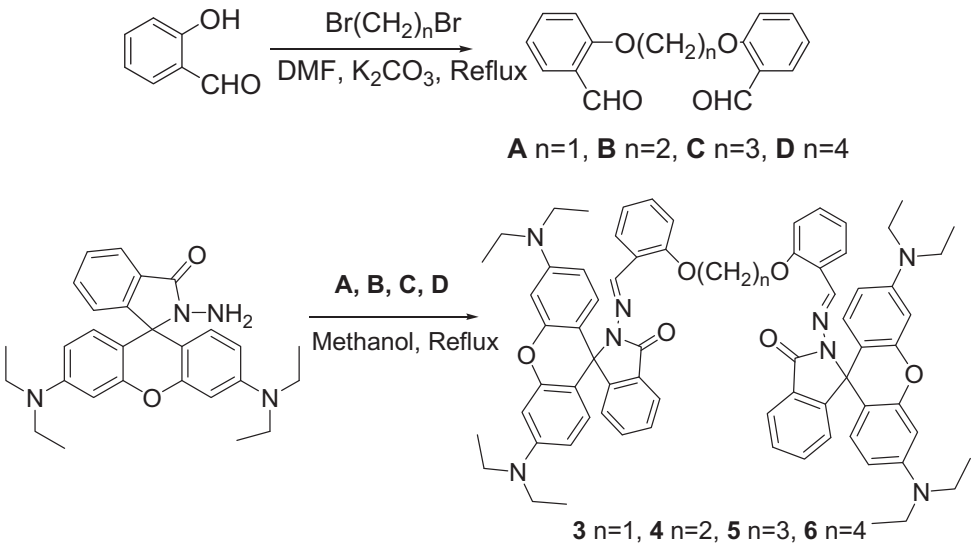

Scheme 2. Synthesis of bis-rhodamine based chemosensors **3**–**6.**

HCl–CH_3CN pH 7.4 were colorless and did not show any absorbance in 500–600 nm region. However, addition of either Cu^{2+} or Fe^{3+} ions (50 μM) induced a new peak centered at ~ 555 nm with a shoulder peak at 520 nm. Other competitive metal ions did not influence the absorption characteristics of **1** and **2**. The enhancement in the absorbance of **1** upon addition of Cu^{2+} and Fe^{3+} were 53 and 57 fold respectively, and indicated that **1** had nearly equal sensitivity for both Cu^{2+} and Fe^{3+}. However, the enhancement factor of absorbance of **2** upon addition of Cu^{2+} and Fe^{3+} were 38 and 154, respectively. This observation indicated that the furan O-atom in **2** could favor the binding of Fe^{3+} ions over Cu^{2+} ions. It was also clear from Job plot (Supporting data, Fig. S11–S12) that both chemosensors **1** and **2** formed complexes with Cu^{2+} and Fe^{3+} ions in 2:1 stoichiometry (Supporting data, Scheme 1). Thus, the observed selectivity for Fe^{3+} over Cu^{2+} in the case of **2** could be explained in terms of the theory of hard and soft acids and bases (HSAB theory). The furan O-atom in **2** being a stronger hard base than the pyridine N-atom in **1**, the former is likely to form a more stable complex with Fe^{3+} (a stronger hard acid as compared to Cu^{2+}) than the latter. Moreover, it seems likely that compared to the chelating ligand of **1** that contains O–N–N combination of donor atoms, the chelating ligand of relatively rigid molecule **2** containing O–N–O combination of donor atoms might fit better with Fe^{3+} than with Cu^{2+}.

As regards the origin of metal ion selectivity, higher negative charge of the ligand and higher number of chelate rings, greatly increase the stabilities of the metal chelates formed, but decrease selectivity [53]. Chelate effect which originates from the difference in entropy between chelate and non-chelate complex reactions significantly influences metal ion selective chelation [54]. In the case of rhodamine derivatives, even a slight change in the steric requirement or puckering of chelating ring drastically alters metal-donor atom interactions and completely change the metal ion selectivity [50,55–60]. Achievement of such steric effects requires considerable rigidity in the ligand. The rigid positioning of donor atoms in a ligand (the O–N–O combination of donor atoms in the present study), can best be obtained in aromatic ligands as compared with aliphatic analogs.

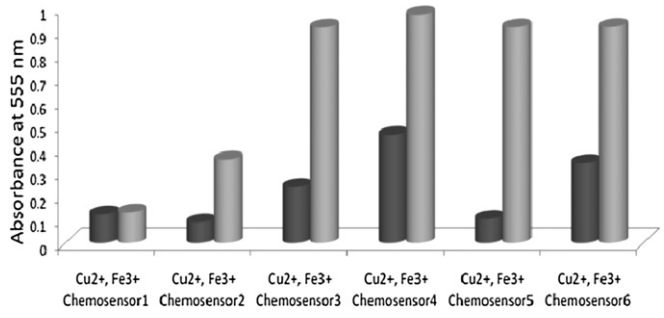

Fig. 1. Relative sensitivities of chemosensors (10 μM) to Cu^{2+} (50 μM) and Fe^{3+} (50 μM) ions.

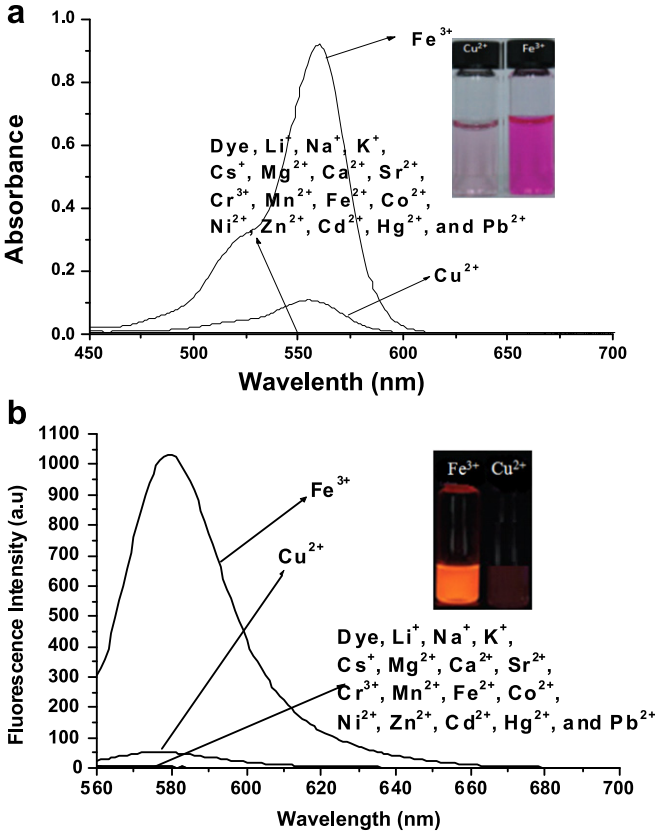

Fig. 2. Comparison of absorbance (a) and fluorescence (b) characteristics of **5** (10 μM) in 1:1 v/v 0.01 M Tris HCl–CH_3CN pH 7.4 in response to different metal ions (50 μM).

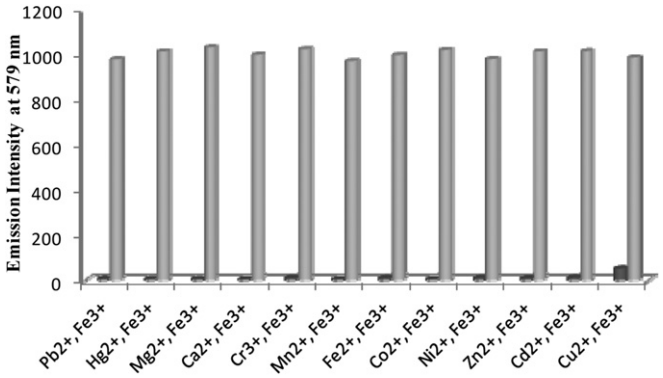

Fig. 3. Metal-ion selectivity of **5** (10 μM) in 1:1 v/v 0.01 M Tris HCl–CH_3CN pH 7.4. The dark bars represent the fluorescence emission of a solution of **5** (10 μM) and 5 equiv of the cation of interest. The light bars show the fluorescence change that occurs upon addition of 1 equiv of Fe(III) to the solution containing **5** (10 μM)and the cation (50 μM).

In our previous work we successfully demonstrated that a bisrhodamine chemosensor was more sensitive than its monorhodamine analog [51]. Based on the observed selectivity for Fe^{3+} over Cu^{2+} in the case of **2** and the results of our previous work, we speculated that the spatial disposition of O–N–O donor atoms combined with an appropriate spacer in a bis-rhodamine analog would result in a sensor with enhanced sensitivity and selectivity for Fe^{3+} ions. Such a chemosensor should form a complex with Fe^{3+} ion in 1:1 stoichiometry as opposed to the 2:1 stoichiometry observed for **2**. Accordingly, four bis-rhodamine probes **3**, **4**, **5** and **6** with similar coordinating moieties and incremental spacer lengths were synthesized as shown in Scheme 2 and characterized by NMR and Mass analyses (Supporting data, Fig. S13–S24). Despite the presence of two rhodamine moieties, all four bis-rhodamine probes **3**–**6** gave a colorless solution in 1:1 v/v 0.01 M Tris HCl–CH_3CN pH 7.4 as well as other organic solvents, indicating their spirocyclic structure. The non-fluorescent spirocyclic form of **3**, **4**, **5** and **6** was further confirmed by ^{13}C NMR analysis. While all four bis-rhodamine probes **3**–**6** (10 μM each) were colorless and insensitive to 50 μM concentration of different metal ions (Li^+, Na^+, K^+, Cs^+, Mg^{2+}, Ca^{2+}, Sr^{2+}, Cr^{3+}, Mn^{2+}, Fe^{2+}, Co^{2+}, Ni^{2+}, Zn^{2+}, Cd^{2+}, Hg^{2+}, and Pb^{2+}), they showed the characteristic color only to Fe^{3+} and Cu^{2+} ions (Fig. 1 and Supporting data, Fig. S25). The UV–Visible absorption patterns of **3**–**6** were measured in 1:1 v/v 0.01 M Tris HCl–CH_3CN pH 7.4. Solutions of all four bis-rhodamine probes **3**–**6** did not show any absorbance above 500 nm. But, addition of 50 μM of either Cu^{2+} or Fe^{3+} induced a new peak centered at ~555 nm with a shoulder peak at 520 nm. Other competitive metal ions did not influence the absorption characteristics of **3**–**6** (Supporting data, Fig. S25). Predictably, all the four bis-rhodamine probes **3**–**6** showed nearly equal enhancement (400–407 fold increase) in the absorbance intensity upon addition of Fe^{3+} ions. Under identical conditions the enhancement factors of absorbance of **3, 4, 5** and **6** for Cu^{2+} were 99, 209, 49, and 150, respectively. This remarkable reduction in Cu^{2+} induced absorbance of bis-rhodamine probes **3**–**6** could be ascribed to the low affinity of chelating ligands for Cu^{2+} which in turn would

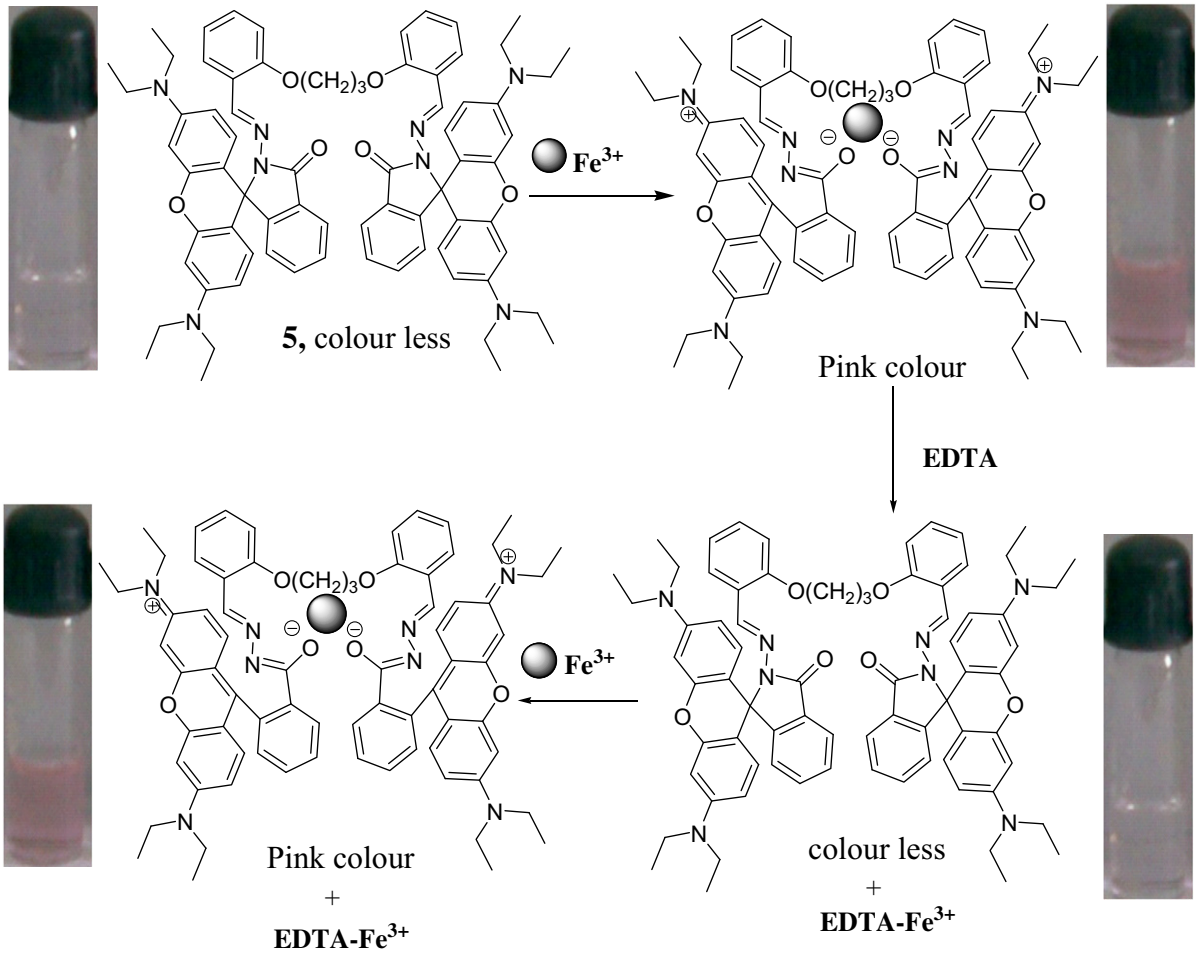

Scheme 3. Perspective mechanism of **5**-Fe^{3+} complex formation.

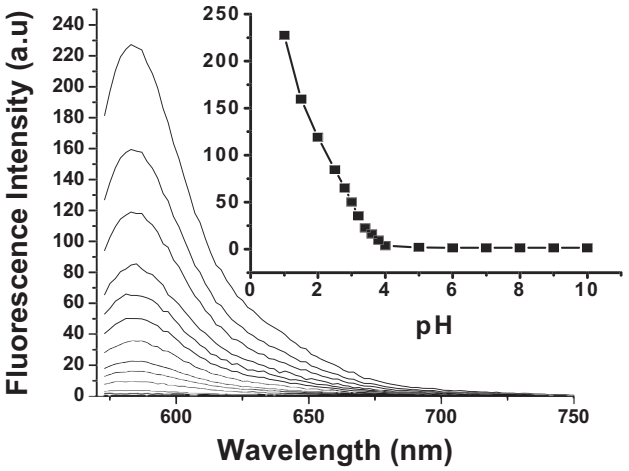

Fig. 4. pH dependant variation in fluorescence intensity of chemosensor **5** (5 μM).

contribute to the selectivity for Fe^{3+} ions (Fig. 1 and Supporting data, Fig. S25). Unlike the mono-rhodamine probes **1** and **2**, the bis-rhodamine probes **3**–**6**, formed complexes with Fe^{3+} and Cu^{2+} ions in 1:1 stoichiometry as determined by Job plot (Supporting data, Fig. S26–S29). As it is apparent that all four bis-rhodamine probes **3**–**6** contain the same O–N–O combination of donor atoms, the selectivity displayed by **5** (Fig. 2a) can only be ascribed to the spacer length that appears to provide the required chelating ring size and flexibility and, thereby, favor the formation of the complex with Fe^{3+} rather than with Cu^{2+}.

The fluorescence characteristics of **5** were studied in 1:1 v/v 0.01 M Tris HCl–CH_3CN pH 7.4. In the absence of metal ions, **5** alone was fluorescently inactive in the rhodamine emission range (550–650 nm) indicating the existence of the spirocyclic form. The metal ion dependent variations in the fluorescence emission intensity of **5** is shown in Fig. 2b. The fluorescence emission of **5** was highly enhanced upon injection of Fe^{3+} ions. Other competitive metal ions did not show any considerable influence except Cu^{2+} which showed little interference. Interestingly, the fluorescence enhancement factors of **5** (10 μM) for Fe^{3+} and Cu^{2+} ions (10 μM each) were 446 and 23, respectively (Fig. 2b). Thus, owing to the reduced affinity of the bis-rhodamine probe **5** for Cu^{2+} ions, Fe^{3+} ions could be selectively detected. The concentration dependant variations in the fluorescence emission intensity of **5** upon addition of Fe^{3+} and Cu^{2+} ions are shown in the Fig. S30 (Supporting data). Addition of incremental concentrations of Fe^{3+} induced a new emission ~579 nm. The limit of detection of **5** for Fe^{3+} ions was 4×10^{-7} M ($^5I_{4 \times 10^{-7}}/^5I_0 = 4.25$) [50]. The metal competition assay carried out by adding Fe^{3+} ions (10 μM) to **5** (10 μM) in the presence of other metal ions (50 μM) revealed that the commonly coexistent metal ions did not show any interference on the Fe^{3+} induced fluorescence emission of **5** as shown in Fig. 3. Only Cu^{2+} induces a little fluorescence emission but addition of Fe^{3+} to the solution of **5**-Cu^{2+} complex leads to a greater enhancement in the fluorescence emission of **5** indicating the high binding affinity of **5** for Fe^{3+} and, suggests that **5** can be used to detect Fe^{3+} even in the presence of Cu^{2+} at high concentrations. Since the concentrations of Cu^{2+} ions are lower than those of Fe^{3+} ions in biological tissues, and the fact that **5** displays a lower affinity for Cu^{2+} ions, the presence of Fe^{3+} ions in biological tissues could be selectively detected using **5**.

The mechanism for the changes in the fluorescence characteristics of **5** upon addition of Fe^{3+} ions is shown in the Scheme 3. As it would be expected, the Fe^{3+} binds with **5**, and opens the spirolactam ring that results in the fluorescence enhancement and development of pink color (Supporting data, Fig. S31). The pink color formed by the addition of Fe^{3+} ions becomes colorless upon addition of EDTA, confirming the reversibility of complex formation and the formation of **5** (Supporting data, Fig. S32). This colorless solution regains its pink color upon addition of excess Fe^{3+} ions, suggesting that the color development is due to the formation **5**-Fe^{3+} complex and not due to any catalytic action of Fe^{3+} ions. Such a complex formation should involve the carbonyl oxygen atom of **5**. The ^{13}C NMR spectra of **5** recorded in the presence of different concentrations of Fe^{3+} ions clearly show the involvement of carbonyl oxygen of **5** in complex formation. The reduction in the ^{13}C-resonance at 66.12 ppm confirms the opening of spirolactam ring upon complex formation with Fe^{3+} ions (Supporting data, Fig. S33). The formation a distorted octahedral complex is supported by theoretical calculations (Supporting data, Fig. S34) and in agreement with the observed spectrometric evidence.

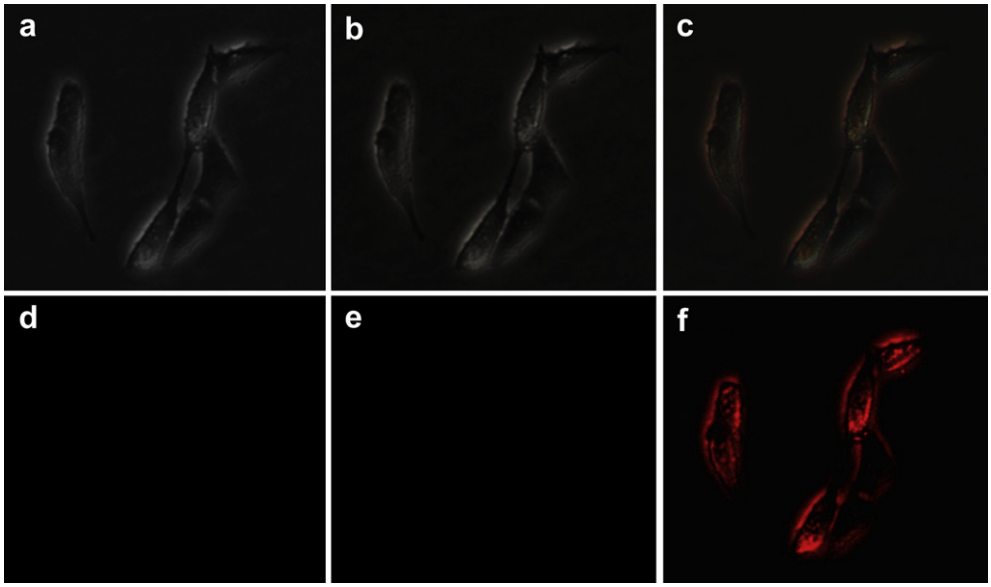

Fig. 5. Microscopic images of (a) untreated fibroblast cells, (b) cells incubated with **5** (1 μM), (c) cells incubated with **5** (1 μM) and Fe^{3+} (5 μM), and, fluorescence microscopic images of (d) untreated cells, (e) cells incubated with **5** (1 μM), and (f) cells incubated with **5** (1 μM) and Fe^{3+} (5 μM).

The stability at physiological pH is a prerequisite for any chemosensor to be considered for bio-imaging applications. Moreover, chemosensors containing nitrogen donors are highly sensitive to environmental pH as the protonation degree of the nitrogen are strongly dependent on the pH. To verify the stability of chemosensor **5** over a physiologically relevant pH range, fluorescence emission spectra were recorded in the pH range 1–10. Providentially, chemosensor **5** was non-fluorescent within the pH range 5–10, and exhibited considerable level of fluorescence only below pH 4.0 as shown in Fig. 4. This observation suggested that the spirolactam ring in chemosensor **5** was stable above pH 4.0, and chemosensor **5** could be used for sensing Fe^{3+} ions in biological samples.

As a logical extension, we tested the suitability of chemosensor **5** in the imaging of fibroblast cells exposed to Fe^{3+} ions. Mouse fibroblast cell line, NIH 3T3 was incubated with Fe^{3+} ions (5 μM) in Dulbecco's Modified Eagle Medium (DMEM culture medium) for 2 min at 37 °C, and washed with PBS buffer (pH 7.4) to remove excess metal ions. The cells were then treated with chemosensor **5** (1 μM) in the culture medium for 30 min at 37 °C, and then washed with PBS buffer (pH 7.4) to remove unbound chemosensor. From a 100 μM stock solution of **5** in 1:1 CH_3CN-buffer, 10 μL was dispersed into 1 mL culture medium to obtain a final concentration of 1 μM of **5** (0.5% CH_3CN in DMEM medium) in order to minimize the effect of CH_3CN. Fibroblast cells treated with both chemosensor **5** and Fe^{3+} displayed intense red fluorescence as shown in Fig. 5. The normal and fluorescence microscopic images clearly indicated that chemosensor **5** could be used to detect live fibroblast cells exposed to micro molar concentrations of Fe^{3+} ions. Fibroblast cells not exposed to Fe^{3+} ions did not show any fluorescence, suggesting the suitability of chemosensor **5** for bio-imaging applications.

4. Conclusion

In conclusion, the effect of the number and nature of coordinating sites and spatial disposition of chelating moieties for the selective recognition of Fe^{3+} ions are demonstrated. The significance of chelating ring size and the rigid positioning of O–N–O combination of donor atoms in a chelating ligand for Fe^{3+} selective chelation is also illustrated. In addition, the protocol for the synthesis of six new rhodamine based chemosensors is reported. Taking advantage of the fluorescence properties of the chemosensor **5**, a possible application of **5** in the imaging of live fibroblast cells exposed to toxic Fe^{3+} ions in aqueous samples is also presented.

Acknowledgments

We thank D. Muralidharan, Organic Chemistry Division, CLRI, Chennai, for his critical suggestions on this manuscript. Two of the authors Ch. N. R and K. S. thank the Council of Scientific and Industrial Research (CSIR), New Delhi, India for the research fellowship.

Appendix A. Supplementary material

The ^1H NMR, ^{13}C NMR, and Mass analytical data, and fluorescence and absorbance spectra of chemosensors, as well as Job plots are provided in Supplementary Material. ^1H- and ^{13}C NMR spectra of rhodamine hydrazide and bis-salicyladehyde derivatives are also included. Supplementary material associated with this article can be found, in the online version, at http://dx.doi.org/10.1016/j.dyepig.2012.05.025.

References

[1] Meneghini R. Iron homeostasis, oxidative stress, and DNA damage. Free Radic Biol Med 1997;23:783–92.
[2] Aisen P, Wessling-Resnick M, Leibold EA. Iron metabolism. Curr Opin Chem Biol 1999;3:200–6.
[3] Eisenstein RS. Iron regulatory proteins and the molecular control of mammalian iron metabolism. Annu Rev Nutr 2000;20:627–62.
[4] Rouault TA. The role of iron regulatory proteins in mammalian iron homeostasis and disease. Nat Chem Biol 2006;2:406–14.
[5] Brugnara C. Iron deficiency and erythropoiesis: new diagnostic approaches. Clin Chem 2003;49:1573–8.
[6] Ohashi A, Ito H, Kanai C, Imura H, Ohashi K. Cloud point extraction of iron(III) and vanadium(V) using 8-quinolinol derivatives and triton X-100 and determination of 10^{-7} mol dm^{-3} level iron(III) in riverine water reference by a graphite furnace atomic absorption spectroscopy. Talanta 2005;65:525–30.
[7] Liang Z-Q, Wang C-X, Yang J-X, Gao H-W, Tiang Y-P, Tao X-T, et al. A highly selective colorimetric chemosensor for detecting the respective amounts of iron(II) and iron(III) ions in water. New J Chem 2007;31:906–10.
[8] Lunvongsa S, Oshima M, Motomizu S. Determination of total and dissolved amount of iron in water samples using catalytic spectrophotometric flow injection analysis. Talanta 2006;68:969–73.
[9] Tesfaldet ZO, van Staden JF, Stefan RI. Sequential injection spectrophotometric determination of iron as Fe(II) in multi-vitamin preparations using 1,10-phenanthroline as complexing agent. Talanta 2004;64:1189–95.
[10] Gomes DMC, Segundo MA, Lima JLFC, Rangel AOSS. Spectrophotometric determination of iron and boron in soil extracts using a multi-syringe flow injection system. Talanta 2005;66:703–11.
[11] Bobrowski A, Nowak K, Zarebski J. Application of a bismuth film electrode to the voltammetric determination of trace iron using a Fe(III)–TEA–-BrO_3^- catalytic system. Anal Bioanal Chem 2005;382:1691–7.
[12] Ramette RW, Sandell EB. Rhodamine B equilibria. J Am Chem Soc 1956;78:4872–8.
[13] Prodi L, Bolletta F, Montalti M, Zaccheroni N. Luminescent chemosensors for transition metal ions. Coord Chem Rev 2000;205:59–83.
[14] Valeur B, Leray I. Design principles of fluorescent molecular sensors for cation recognition. Coord Chem Rev 2000;205:3–40.
[15] Chen X, Pradhan T, Wang F, Kim JS, Yoon J. Fluorescent chemosensors based on spiroring-opening of xanthenes and related derivatives. Chem Rev 2012;112:1910–56.
[16] Beija M, Afonso CAM, Martinho JMG. Synthesis and applications of rhodamine derivatives as fluorescent probes. Chem Soc Rev 2009;38:2410–33.
[17] Kim HN, Lee MH, Kim HJ, Kim JS, Yoon J. A new trend in rhodamine-based chemosensors: application of spirolactam ring-opening to sensing ions. Chem Soc Rev 2008;37:1465–72.
[18] Zou Q, Li X, Zhang J, Zhou J, Sun B, Tian H. Unsymmetrical diarylethenes as molecular keypad locks with tunable photochromism and fluorescence via Cu^{2+} and CN^- coordinations. Chem Commun 2012:2095–7.
[19] Kim HN, Guo Z, Zhu W, Yoon J, Tian H. Recent progress on polymer-based fluorescent and colorimetric chemosensors. Chem Soc Rev 2011:79–93.
[20] Kumar M, Kumar R, Bhalla V. 'On–Off' reversible switch for Fe^{3+} and F^- mimicking XNOR logic function. Tetrahedron Lett 2010;51:5559–62.
[21] Li Z, Zhang L, Li X, Guo Y, Ni Z, Chen J, et al. A fluorescent color/intensity changed chemosensor for Fe^{3+} by photo-induced electron transfer (PET) inhibition of fluoranthene derivative. Dyes Pigm 2012;94:60–5.
[22] Zhang L, Wang J, Fan J, Guo K, Peng X. A highly selective, fluorescent chemosensor for bioimaging of Fe^{3+}. Bioorg Med Chem Lett 2011;21:5413–6.
[23] Queirós C, Silva AMG, Lopes SC, Ivanova G, Gameiro P, Rangel M. A novel fluorescein-based dye containing a catechol chelating unit to sense iron(III). Dyes Pigm 2012;93:1447–55.
[24] Mansell D, Rattray N, Etchells LL, Schwalbe CH, Blake AJ, Bichenkova EV, et al. Fluorescent probe: complexation of $Fe^{3+}$with the *myo*-inositol 1,2,3-trisphosphate motif. Chem Commun 2008:5161–3.
[25] Lin W, Yuan L, Feng J, Cao X. A fluorescence-enhanced chemodosimeter for Fe^{3+} based on hydrolysis of bis(coumarinyl) schiff base. Eur J Org Chem 2008:2689–92.
[26] Li Z-X, Zhang L-F, Zhao W-Y, Li X-Y, Guo Y-K, Yu M-M, et al. Fluoranthene-based pyridine as fluorescent chemosensor for Fe^{3+}. Inorg Chem Commun 2011;14:1656–8.
[27] Lee DY, Singh N, Jang DO. A benzimidazole-based single molecular multi-analyte fluorescent probe for the simultaneous analysis of Cu^{2+} and Fe^{3+}. Tetrahedron Lett 2010;51:1103–6.
[28] Zhan J, Wen L, Miao F, Tian D, Zhu X, Li H. New J Chem 2012;36:656–61.
[29] Xu M, Wu S, Zeng F, Yu C. Cyclodextrin supramolecular complex as a water-soluble Ratiometric sensor for Ferric ion sensing. Langmuir 2010;26:4529–34.
[30] Kumar M, Kumar R, Bhalla V, Sharma PR, Kaur T, Qurishi Y. Thiacalix[4]arene based fluorescent probe for sensing and imaging of Fe^{3+} ions. Dalton Trans 2012;41:408–12.
[31] Ouchetto H, Dias M, Mornet R, Lesuissec E, Camadro J-M. A new route to trihydroxamate-containing artificial siderophores and synthesis of a new fluorescent probe. Bioorg Med Chem 2005;13:1799–803.
[32] Qin C, Cheng Y, Wang L, Jing X, Wang F. Phosphonate-functionalized polyfluorene as a highly water-soluble iron(III) chemosensor. Macromolecules 2008;41:7798–804.

[33] Weerasinghe AJ, Schmiesing C, Varaganti S, Ramakrishna G, Sinn E. Single- and multiphoton turn-on fluorescent Fe^{3+} sensors based on bis(rhodamine). J Phys Chem B 2010;114:9413–9.
[34] Hao E, Meng T, Zhang M, Pang W, Zhou Y, Jiao L. Solvent dependent fluorescent properties of a 1,2,3-triazole linked 8-hydroxyquinoline chemosensor: tunable detection from zinc(II) to iron(III) in the CH_3CN/H_2O system. J Phys Chem A 2011;115:8234–41.
[35] Yina W, Cuia H, Yanga Z, Li C, She M, Yina B, et al. Facile synthesis and characterization of rhodamine-based colorimetric and "off–on" fluorescent chemosensor for Fe^{3+}. Sensors and Actuators B 2011;157:675–80.
[36] Donga L, Wua C, Zenga X, Mua L, Xuea S-F, Taoa Z, et al. The synthesis of a rhodamine B schiff-base chemosensor and recognition properties for Fe^{3+} in neutral ethanol aqueous solution. Sensors and Actuators B 2010;145:433–7.
[37] Hu Z-Q, Feng Y-C, Huang H-Q, Ding L, Wang X-M, Lin C-S, et al. Fe^{3+}-selective fluorescent probe based on rhodamine B and its application in bioimaging. Sensors and Actuators B 2011;156:428–32.
[38] Xiang Y, Tong A. A new rhodamine-based chemosensor exhibiting selective Fe^{III}-amplified fluorescence. Org Lett 2006;8:1549–52.
[39] She M, Yang Z, Yin B, Zhang J, Gu J, Yin W, et al. A novel rhodamine-based fluorescent and colorimetric "off–on" chemosensor and investigation of the recognizing behavior towards Fe^{3+}. Dyes Pigm 2012;92:1337–43.
[40] Yang Z, She M, Yin B, Cui J, Zhang Y, Sun W, et al. Three rhodamine-based "Off–On" chemosensors with high selectivity and sensitivity for Fe^{3+} imaging in living cells. J Org Chem 2012;77:1143–7.
[41] Mao J, Wang L, Dou W, Tang X, Yan Y, Liu W. Tuning the selectivity of two chemosensors to Fe(III) and Cr(III). Org Lett 2007;9:4567–70.
[42] Lim NC, Pavlova SV, Bruckner C. Squaramide hydroxamate-based chemidosimeter responding to iron(III) with a fluorescence intensity increase. Inorg Chem 2009;48:1173–82.
[43] Sumner JP, Kopelman R. Alexa Fluor 488 as an iron sensing molecule and its application in PEBBLE nanosensors. Analyst 2005;130:528–33.
[44] Zhang X, Shiraishi Y, Hirai T. A new rhodamine-based fluorescent chemosensor for transition metal cations synthesized by one-step facile condensation. Tetrahedron Lett 2007;48:5455–9.
[45] Wolf C, Mei X, Rokadia HK. Selective detection of Fe(III) ions in aqueous solution with a 1,8-diacridylnaphthalene-derived fluorosensor. Tetrahedron Lett 2004;45:7867–71.
[46] Bricks JL, Kovalchuk A, Trieflinger C, Nofz M, Buschel M, Tolmachev AI, et al. On the development of sensor molecules that display Fe^{III}-amplified fluorescence. J Am Chem Soc 2005;127:13522–9.
[47] Ma Y, Luo W, Quinn PJ, Liu Z, Hider RC. Design, synthesis, physicochemical properties, and evaluation of novel iron chelators with fluorescent sensors. J Med Chem 2004;47:6349–62.
[48] Wu X, Xu B, Tong H, Wang L. Phosphonate-functionalized polyfluorene film sensors for sensitive detection of iron(III) in both organic and aqueous media. Macromolecules 2010;43:8917–23.
[49] De Silva AP, Gunarante HQN, Gunnlaugsson T, Huxley AJM, McCoy CP, Rademacher JT, et al. Signaling recognition events with fluorescent sensors and switches. Chem Rev 1997;97:1515–66.
[50] Zhao Y, Zhang X-B, Han Z-X, Qiao L, Li C-Y, Jian L-X, et al. Highly sensitive and selective colorimetric and Off–On fluorescent chemosensor for Cu^{2+} in aqueous solution and living cells. Anal Chem 2009;81:7022–30.
[51] Narendra Reddy Ch, Thennarasu S. Synthesis of a highly selective bis-rhodamine chemosensor for naked-eye detection of Cu^{2+} ions and its application in bio-imaging. Dyes and Pigments 2011;91:378–82.
[52] Valeur B. Molecular fluorescence: principles and applications. New York: Wiley-VCH Verlag GmbH; 2001. ch. 10.
[53] Hancock RD, Martell AE. Ligand design for selective complexation of metal ions in aqueous solution. Chem Rev 1989;89:1875–914.
[54] Hay BP, Zhang D, Rustad JR. Structural criteria for the rational design of selective ligands. 2. Effect of alkyl substitution on metal ion complex stability with ligands bearing ethylene-bridged ether donors. Inorg Chem 1996;35: 2650–8.
[55] Chen X, Jia J, Ma H, Wang S, Wang X. Characterization of rhodamine B hydroxylamide as a highly selective and sensitive fluorescence probe for copper(II). Analytica Chimica Acta 2009;632:9–14.
[56] Bae S, Tae J. Rhodamine-hydroxamate-based fluorescent chemosensor for Fe^{III}. Tetrahedron Lett 2007;48:5389–92.
[57] Huang L, Wang X, Xie G, Xi P, Li Z, Xu M, et al. A new rhodamine-based chemosensor for Cu^{2+} and the study of its behaviour in living cells. Dalton Trans 2010:7894–6.
[58] Wu D, Huang W, Duan C, Lin Z, Meng Q. Highly sensitive fluorescent probe for selective detection of Hg^{2+} in DMF aqueous media. Inorg Chem 2007;46: 1538–40.
[59] Huang W, Zhu X, Wua D, He C, Hu X, Duan C. Structural modification of rhodamine-based sensors toward highly selective mercury detection in mixed organic/aqueous media. Dalton Trans 2009:10457–65.
[60] Suresh M, Mishra S, Mishra SK, Suresh E, Mandal AK, Shrivastav A, et al. Resonance energy transfer approach and a new ratiometric probe for Hg^{2+} in aqueous media and living organism. Org Lett 2009;11:2740–3.